Hindawi
Journal of Nanomaterials
Volume 2022, Article ID 9649711, 11 pages
https://doi.org/10.1155/2022/9649711

Research Article

Investigation on Dye Regeneration Kinetics at P-Type Sensitized Nanoparticle Nickel Oxide Film by Scanning Electrochemical Microscopy

Getachew Alemu Anshebo and Ataklti Abraha Gebreyohanes

College of Natural and Computational Sciences, Department of Physics, Samara University, Samara, Ethiopia

Correspondence should be addressed to Ataklti Abraha Gebreyohanes; atklt.physics@gmail.com

Received 15 March 2022; Accepted 27 June 2022; Published 18 July 2022

Academic Editor: Lavinia Balan

The efficiency of a NiO-sensitized solar cell is determined by the kinetics of hole injection and dye regeneration reactions at the NiO/dye/electrolyte interface. In this research, the photochemical regeneration kinetics of dye adsorbed on the NiO film was investigated by scanning electrochemical microscopy (SECM). Besides, organic C343 and P1 sensitizers in combination with iodide-based, cobalt-based, and thiolate-based electrolytes were selected to understand the effect of sensitizers and redox shuttles on the dye regeneration process. As a result, a fast regeneration kinetic rate constant was conformed in the thiolate-based sample compared with cobalt-based and iodide-based, demonstrating that the organic redox shuttle was an efficient mediator to optimize the performance of p-type DSSC. Furthermore, the regeneration rate constants (k_{eff}), reduction rate constants (k_{red}), and absorption cross section (Φ_{hv}) were investigated for organic dyes and electrolytes. That is, an effective dye regeneration rate constant k_{red} of $6.95 \times 10^5\ \text{mol}^{-1}\text{cm}^3\text{s}^{-1}$ for NiO/P1 and k_{red} of $3.75 \times 10^5\ \text{mol}^{-1}\text{cm}^3\text{s}^{-1}$ for NiO/C343 was found at various wavelengths. Therefore, the experimental results demonstrate that regeneration kinetics are dependent on the type of electrolyte and dye used. Moreover, the results suggest that scanning electrochemical microscopy is a powerful method for screening efficient dyes and electrolytes for charge transfer reactions in P-type dye-sensitized solar cells.

1. Introduction

Due to their low production cost, versatility, low toxicity, and competitive light-to-electric energy efficiency compared to silicon solar cells, dye-sensitized solar cells (DSSC) have recently gotten a lot of attention [1–4]. As an emerging PV, dye-sensitized solar cells (DSSCs) can advance the energy produced from renewable sources and energy efficiency through their applications. Until recently, a variety of studies on the sensitization of n-type titanium dioxide (TiO2) and zinc oxide (ZnO) have been conducted [5, 6]. The progress of solar cell conversion efficiency was 7% [1], and Nazeeruddin's team's effort increased it to around 10% [7]. Nowadays, the best laboratory-scale confirmed result is 12.3% [8], which is slightly lower than the highest efficiency reported by Kakiage et al. of around 14% [9].

Currently, a new type of DSSC has evolved as a new solar cell based on the p-type semiconductor (p-SC) where the photoexcited dyes (HOMO) are reductively quenched by hole injection into the semiconductor's valence band [10, 11]. The excited dye (D^*) injects a hole into the semiconductor's valence band (VB) upon light absorption, resulting in dye reduction (D^-). The injected holes diffuse to the back transparent conducting electrode (TCO), which then passes via the external circuit to reach the counter electrode [12–14]. In this perspective, the nickel oxide nonmaterial is the predominant p-SC material used, but much higher photo conversion efficiencies and it is applicable in several applications are needed [15–19].

In preceding studies, researchers have analyzed the effect of electrolytes on dye regeneration for the reason that charge transfer kinetics are very much associated with the photovoltaic

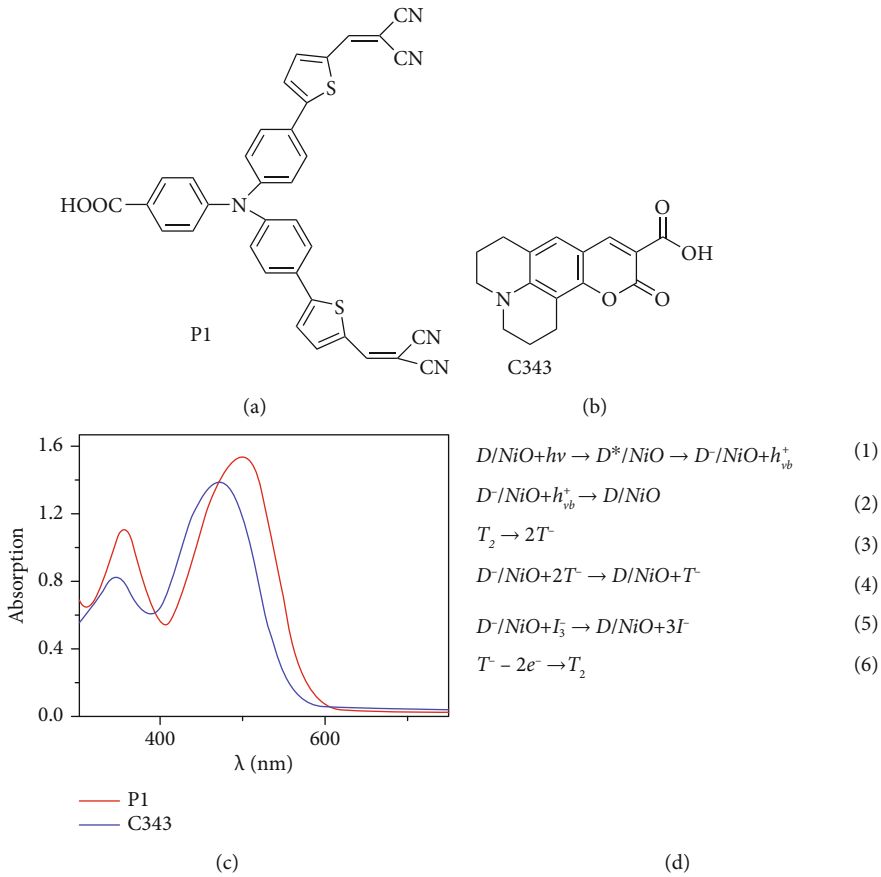

FIGURE 1: The molecular structure of (a) P1 sensitizer, (b) C343, and (c) absorption spectra of P1 and C343 dyes (d) light-induced electron transfer reactions in p-type DSCs. D^-: the reduced dye; hvb+: holes in the valence band of the semiconductor. Electrolyte redox potentials and the valence band edge of NiO [16, 17, 39].

performance of DSSC devices [12, 20, 21]. In the past few decades, a comprehensive investigation into the dye regeneration mechanism in DSSCs has been performed by transient absorption spectroscopy [22]. SECM, which has a wide range of applications in biological processes [23], living cell studies [24], batteries [25], fuel cells [26], quantum dots [27], supercapacitors [28], and solar cells [29], was recently used to investigate the regeneration kinetics of redox couples and an organometalic halide perovskite [30]. And, it has been shown to be a useful tool for studying electron transfer kinetics across a variety of interfaces, including polymer/liquid [31, 32], liquid/liquid interface [33], and redox enzymes [34]. In this study, we provide an experimental investigation on the regeneration kinetics of P1 (as shown in Figure 1(a)), and C343 (as shown in Figure 1(b)) dyes by using SECM on semiconductor oxides NiO with the three different electrolytes I^-, T^-, and Co^{2+} for comparative study under different illumination wavelengths.

2. Experimental Methods

2.1. Materials. The NiO paste was prepared by ball-milling 4 grams of NiO nanoparticles (with a particle size of 20 nm) in 50 mL of ethanol. Then, to obtain a fine dispersion, the aforementioned colloidal solution, 4.4 gm of EC (30-60 mPas), 5.6 gm of EC (5-15 mPas), ethyl cellulose, and 10 gm of triponal were sonicated and stirred overnight alternately. On a rotary evaporator, the ethanol from the mixture was evaporated to make a paste. And, the FTO glass was coated with nickel acetate ethanol solution (0.05 M) by dip-coating and subsequently dried before screen printing. The photocathode films were screen printed with the NiO paste and cured for 5 min at 125°C [35–38].

2.2. Instruments and Procedures. The SECM apparatus for dye-sensitized solar experiments were used. The SECM experiments were performed on a CHI920C electrochemical workstation (CH Instruments, Shanghai). A homemade Teflon cell with a volume of 2 mL was used to hold a Pt wire counter electrode and an Ag/Ag+ reference electrode. The dye-sensitized NiO film coded as P1/NiO electrodes was placed at the bottom, sealed by an O-ring. Moreover, an extra Pt wire connected the back contact of the NiO/P1 sample with reduced (I^-) electrolyte to operate the photo electrochemical cell in a short-circuit setup. The LEDs were placed close to the dye coated sample from the back side and focused on film electrodes by an objective lens. The LEDs were placed close to the dye-coated sample from the back side and focused on film electrodes by an objective lens incident light power on the illuminated area 0.0785 cm^2 and photon flux density J_{hv} of 2.2×10^{-9} to 22.4×10^{-9}

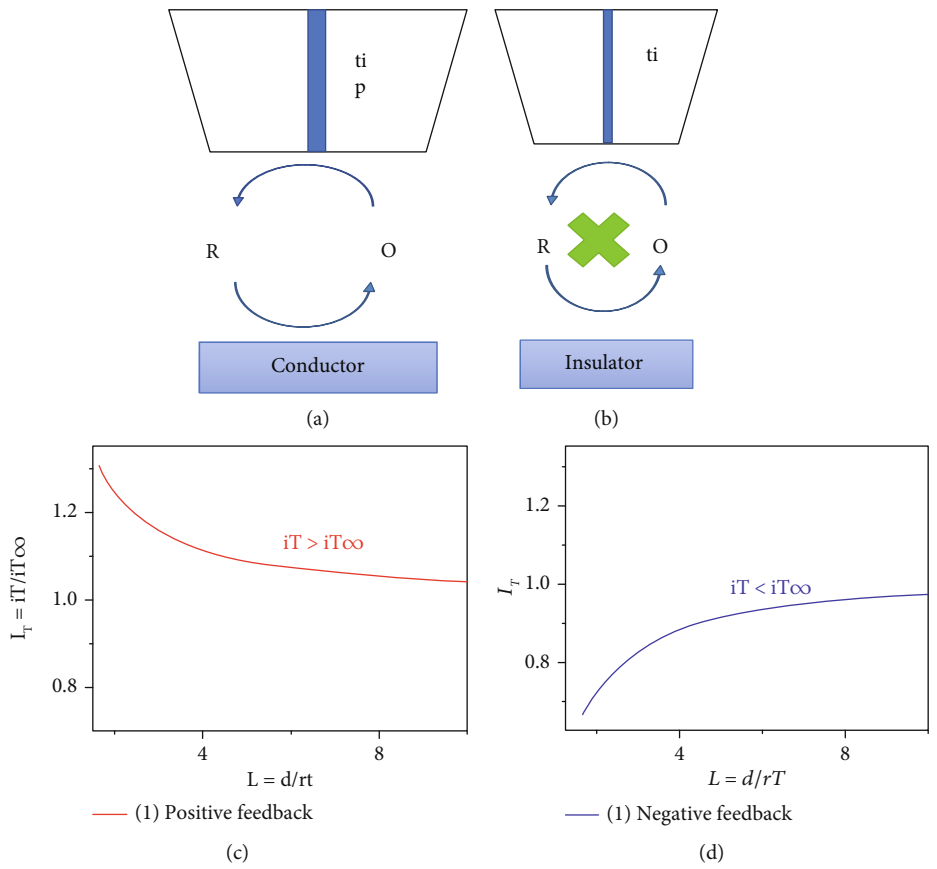

FIGURE 2: Basic principle of the feedback mode (a). Reaction diffuses to the substrate (b). Substrate surface is an insulator (c). Positive feedback (d). Negative feedback.

mol cm^{2}s^{-1} for blue LED and 2.2×10^{-9} to 14.9×10^{-9} mol cm^{2}s^{-1} for red LED. A 25 μm diameter Pt wire (Good Fellow, Cambridge, UK) was sealed into a 5 cm glass capillary prepared by a vertical pull pin instrument (PC-10, Japan). The ultramicroelectrode (UME) was polished by a grinding instrument (EG-400, Japan) and micropolishing cloth with 1.0, 0.3, and 0.05 m alumina powder. The UME was then conically sharpened to an RG of 10, where RG is the ratio of the glass sheath and Pt disk diameters. Then, the approach curves are given as normalized UME current I_T vs. normalized distance L. The position Z max at which mechanical contact of the UME with the sensitized sample and the distance d_o of the active electrode area to the sample at Z max, where L is obtained from the vertical position z increasing with the approach toward the NiO/P1 sample. Therefore, the possible distance between the substrate and tip is 200 μm $\pm$ d_o, the potential at the tip is ET = 0.7 V. The potential of the UME was selected after recording a cyclic voltammetry. ET (using Figure 1(d)) was taken well in the region of the diffusion-controlled oxidation current such that insignificant variations in the reference electrode potential would not change the UME current [34, 39–41].

3. Results and Discussion

3.1. Investigation of SECM Feedback Mode at Various Illuminations. As mentioned in Equation (1a), the SECM feedback mode permits electrochemical currents to collect local quantitative information of oxidation reaction rates. The tip current (I_T) reaches asymptotic conduct with the steady-state current as indicated by Equation (1b).

$$R - ne^- \longrightarrow O, \tag{1a}$$

$$I_{T,\infty} = 4nCF\frac{k_{\text{eff}}}{\kappa}r_T, \tag{1b}$$

where n is the number of electrons transferred at the electrode tip, F denotes Faraday's constant, C denotes the concentration of reduced species, k_{eff} denotes the regeneration rate constant, r_T denotes the radius of the tip, and k denotes the normalized rate constant [34, 39–41]. Figures 2(a) and 2(b) show that basic operation principle on conducting surface and nonconducting/insulator. That is, when the tip moves near to a conductive substrate, the oxidized species formed in reaction (1) diffuse to the substrate and can be reduced back to R and the UME current exceeds the finite distance current ($i_T > i_{T\infty}$), termed "positive feedback," as shown in Figure 2(c). On the other hand, when the tip moves to the substrate surface, which is a nonconducting surface, there is no redox reaction and termed "negative feedback" ($i_T > i_{T\infty}$), as in Figure 2(d) [34, 39–42]. Furthermore, as shown in Equations (2a) and (2b), the analytical equations utilized for the current vs. distance

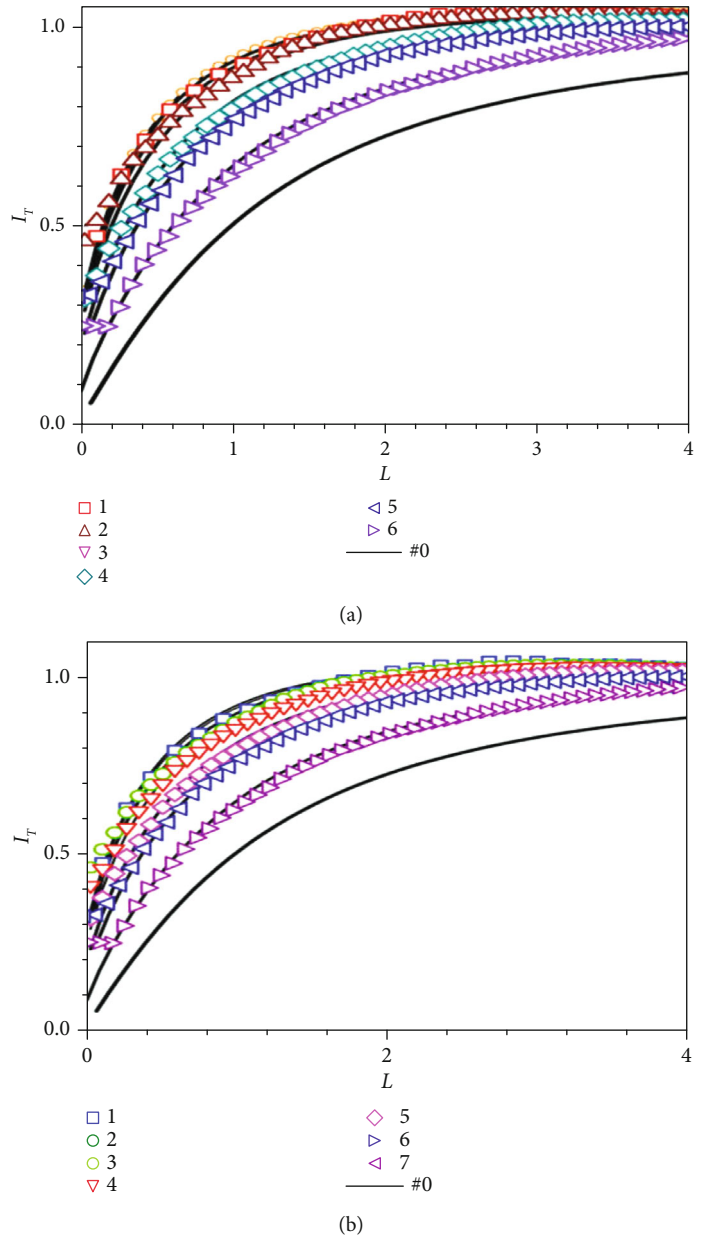

Figure 3: Normalized SECM feedback approach curves of Pt UME towards P1/NiO under illumination by (a) blue LED and (b) red LED.

curves for positive (conductive $I_T{}^{C}$) and negative (insulating, $I_T{}^{ins}$) feedback, respectively. The total tip current is equal to the sum of the steady-state and probe approach currents, as shown in Equation (2c).

$$I_T^C(L) = A + B + C\exp(D/L) = \frac{I_T}{I_{T\infty}}, \tag{2a}$$

$$I_T^{ins}(L) = \frac{1}{A + B + C\exp(D/L)} = \frac{I_T}{I_{T\infty}}, \tag{2b}$$

$$I_{T(L)} = I_{T,ins(L)} + I_{T,\infty} = \frac{I_T}{I_{T,\infty}} + 4nCF\frac{k_{eff}}{\kappa}r_T^2, \tag{2c}$$

where $L = (d/r_T)$ is the normalized tip/substrate distance, and the coefficients A, B, C, and D are fitting constant parameters.

In illumination intensity, the reduced specie of electrolyte forms an oxidized yield when the UME approaches to the sensitized NiO surface and increasing the UME current as shown in Equation (2c) [43, 44]. The electron transport processes, such as light absorption, diffusion of the mediator, and hole transfer at dye-sensitized NiO/electrolyte interface, affect the current vs. distance curves on the sensitized NiO film/electrolyte interface [34, 44].

In order to investigate the influence of light intensity on the regeneration kinetics, the SECM measurements were performed with constant mediator concentration, by varying illumination intensities. Figure 3(a) shows the normalized approach curves on UME approaching NiO/P1 film under

Table 1: Normalized rate constants κ and k_{eff} obtained for the reduction of photoexcited P1 by I^- for different illumination intensities of blue and red LEDs and $(I^-) = 1$ mM + 0.1 M of LiTFS supporting electrolyte, $D = 1.86 \times 10^{-5}$ cm^{2}s^{-1}, $r_T = 12.5\,\mu$m, RG = 10, $k_{eff} = \kappa D/r_T$.

J_{hv} (10^{-9}mol cm^{-2}s^{-1})	Curve#	k	k_{eff} (10^{-3}cms^{-1})
(a) Blue			
22.4	1	0.134	1.44
19.8	2	0.119	1.38
13.9	3	0.108	1.24
11.8	4	0.101	1.16
6.82	5	0.099	0.89
6.12	6	0.096	0.84
2.21	7	0.094	0.42
(b) Red			
14.7	7	0.073	0.67
13.1	6	0.071	0.64
12.1	5	0.063	0.62
9.41	4	0.057	0.56
6.82	3	0.039	0.48
4.19	2	0.024	0.36
2.21	1	0.015	0.23

Table 2: Feedback model reduction rate of the regeneration rate k_{red}, absorption cross-section $\Phi_{hv,}$ and regeneration free energy of P1/NiO, C343/NiO, and three different electrolytes.

Dye	$k_{red}/10^5$ (mol^{-1}cm^{3}s^{-1})	Φ_{hv} (cm^{2}mol^{-1})	[ΔGreg/e^-]eV
P1	6.95	9.34×10^6	0.48
		5.17×10^5	
C343	3.75	3.86×10^6	0.95
		4.51×10^5	
Electrolyte			
I^-	6.83	4.93×10^6	2.78
T^-	7.87	5.92×10^6	2.63
Co^{2+}	5.72	4.27×10^6	2.05

the illumination of blue LEDs. As the photon flux density J_{hv} increased from 2.21×10^{-9}mol cm^{-2}s^{-1} to 22.4×10^{-9}mol cm^{-2}s^{-1}, while the regeneration rate constant k_{eff} increased from 0.42×10^{-3}cms^{-1} to 1.44×10^{-3}cms^{-1}. Figure 3(b) shows the normalized approach curves of red-light emitting diodes. As the flux density J_{hv} increased from 2.21×10^{-9}mol cm^{-2}s^{-1} to 14.7×10^{-9}mol cm^{-2}s^{-1} of blue LEDs their corresponding k_{eff} increased from 0.23×10^{-3}cms^{-1} to 0.67×10^{-3} cms^{-1} as shown in Table 1. The analytical dye reduction rate constant k_{red} as a function of k_{eff}, Φ_{hv}, $\Gamma_D{}^o$, J_{hv}, and [I^-] gives the formula for electron transport at the sample's surface, as

$$k_{red} = \frac{2\phi_{hv} J_{hv} k_{eff}}{6[I^-]k_{eff} - 3\Gamma_{D^o}\Phi_{hv} J_{hv}}, \quad (3)$$

where Φ_{hv} is absorption cross-section, J_{hv} is photon flux density, k_{eff} is regeneration rate constant, and $\Gamma_D{}^o$ is dye content at ground level [34, 39, 42–44]. As shown in Table 2, the P1/NiO sample reduction rate $k_{red} = 6.95 \times 10^6$ mol^{-1}cm^{3}s^{-1}, and $\Phi_{h(\lambda)} = 9.04 \times 10^6$ cm^{2}s^{-1} for the blue LED and $\Phi_{hv(\lambda)} = 4.51 \times 10^5$ cm^{2}s^{-1} for the red LED.

Using absorption spectra of P1 and C343 dyes (as shown in Figure 1(c)), the Lambert Beer's law of Equation (4) was used to calculate the light-harvesting efficiency (LHE) for different dyes loading on the surface of the nickel oxide film of $\Gamma_D = 6.3 \times 10^{-8}$ mol cm^2 and illumination intensities.

$$\mathrm{LHE}(\lambda) = \left(1 - 10^{-\Gamma_D \Phi_{hv}}\right) \times 100\%, \quad (4)$$

where LHE is the absorbance of the film, ΓD is dye loading content, and $\Phi(_{hv})$ photon absorption cross-section (cm^{2}mol^{-1}). Theoretical light-harvesting efficiencies at 467 nm (blue LED) and 647 nm (red LED) were calculated

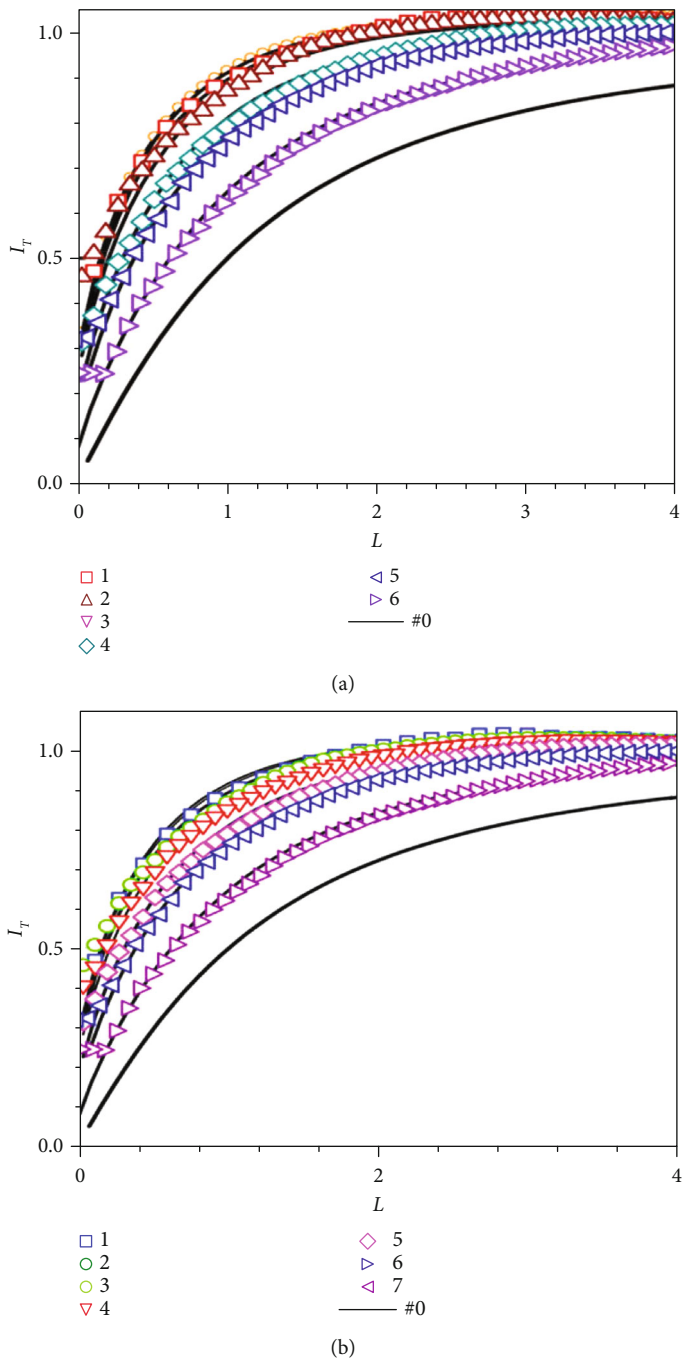

Figure 4: Normalized SECM feedback approach curves of Pt UME towards C343/NiO under illumination by (a) blue LED and (b) red LED.

to be 71.5% and 43%, respectively [40, 43]. The excitation of P1 dye and the emission of blue illumination coincide with high photon absorption [45].

3.2. SECM Feedback Mode Investigation of NiO Films in Different Dyes. To investigate the dependence of the regeneration kinetics on the properties of dyes, we have carried out SECM approach curve measurements on two different dyes, coumarin C343 and P1, at different wavelengths of blue illumination. As photon flux density J_{hv} and k_{eff} increase, the normalized approach curve of UME on C343/NiO film in (blue and red) LED illuminations is shown in Figures 4(a) and 4(b). In blue illumination, k_{eff} increased threefold when photon flux density J_{hv} increased tenfold as shown in Table 3. For C343/NiO, $k_{red} = 3.75 \times 10^5\ mol^{-1}cm^3s^{-1}$, $\Phi_{hv(\lambda)}$, $3.87 \times 10^6\ cm^2s^{-1}$ in blue light and $\Phi_{hv(\lambda)}$,$4.51 \times 10^5\ cm^2s^{-1}$ in red illumination, as illustrated in Table 2. SCEM normalized approach curves of UME towards the C343/NiO and P1/NiO in red illumination are documented in Figure SI-I. Furthermore, the absorption cross-section in blue illumination is higher than in red illumination [36].

Table 3: Normalized rate constants k_{eff} obtained for the reduction of photo excited C343 by I^- for different illumination intensity of blue and red LEDs and $(I^-) = 1\,mM + 0.1\,M$ of LiTFS supporting electrolyte, $D = 1.86 \times 10^{-5}\ cm^2 s^{-1}$, $r_T = 12.5\,lm$, RG = 10, $k_{eff} = kD/r_T$.

J_{hv} (10^{-9}mol cm^{-2} s^{-1})	Curve#	K	k_{eff} (10^{-3}cms^{-1})
Blue			
22.4	1	0.128	1.34
19.8	2	0.111	1.29
13.9	3	0.102	1.15
11.8	4	0.098	1.09
6.82	5	0.096	0.84
6.12	6	0.092	0.79
2.21	7	0.085	0.39
b) Red			
14.7	7	0.083	0.78
13.1	6	0.074	0.71
12.1	5	0.063	0.68
9.41	4	0.059	0.62
6.82	3	0.049	0.53
4.19	2	0.034	0.41
2.21	1	0.022	0.24

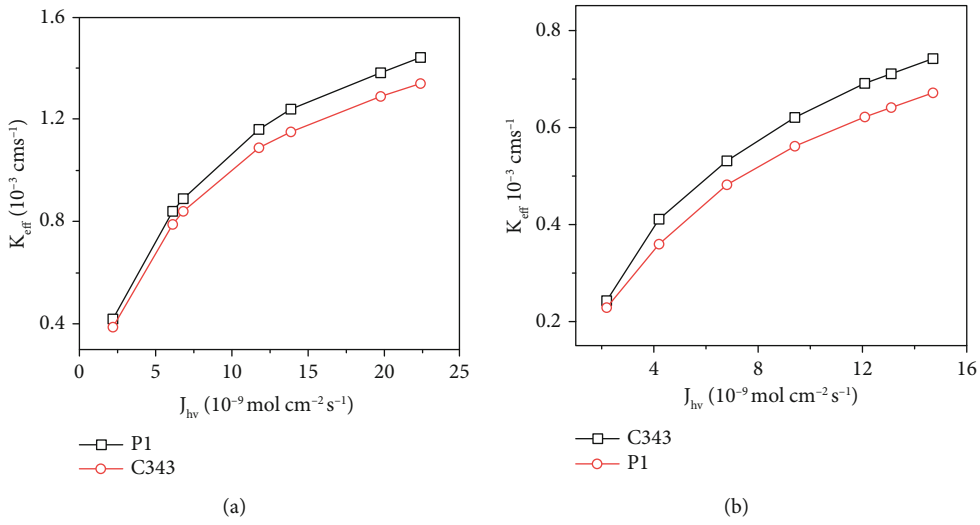

Figure 5: The plot of J_{hv} vs. k_{eff} of NiO/P1 and NiO/C343 under illumination by (a) blue LED and (b) red LED.

Figures 5(a) and 5(b) show the curve of k_{eff} vs. J_{hv} of (P1/NiO and C343/NiO) in blue and red illumination, respectively. As a result, P1/NiO has a higher k_{eff} in blue illumination and a lower k_{eff} in red illumination than C343/NiO. These results were attributed to a shift in the dye's reduction potential from LUMO to the mediator's reduction potential, as represented by [15, 41]

$$\frac{\Delta G^{o}_{reg}}{e^-} = \left(E^{o}\left(\frac{D}{D^-}\right) - E^{O}\left(\frac{I_3^-}{I_2^{\bullet-}}\right)\right), \quad (5)$$

where ΔG^{O}_{reg} stands for regeneration free energies, $E(D/D^-)$ for dye reduction potential, and $E(I_3^-/I_2^{\bullet-}) = -0.35\,V$ vs. NHE for redox reduction potential.

The dye $E(D/D^-)$ has a reduction potential of -0.83 V vs. NHE for P1 dye and -1.2 V vs. NHE for C343 dye. However, there were significant differences in regeneration rate k_{red} and absorption cross-section Φ_{hv} between the two dyes [41]. The free energies of regeneration for P1 dye and C343 dye, according to Equation (5), are -0.48 V vs. NHE and -0.85 V vs. NHE, respectively. As a result, there is a clear variation in the regeneration free energies of different dyes, indicating that the regeneration is highly dependent on dye type [15, 41].

Table 4: Normalized apparent heterogeneous first-order rate constants κ and apparent heterogeneous first-order rate constants k_{eff} obtained from P1/NiO by three different electrolytes T^-, I^-, and Co^{2+} in blue illumination $r_T = 12.5\,\mu m$, RG = 10, $k_{eff} = \kappa D/r_T$.

$J_{hv} \times 10^{-9}$ mol cm^{-2} s^{-1}	Curve #	k	$k_{eff} \times 10^{-3}$cms-1
(a) T^-			
22.4	1	0.13	9.19
19.8	2	0.12	8.91
13.9	3	0.11	8.01
11.8	4	0.109	7.56
6.82	5	0.086	5.93
6.12	6	0.081	5.61
2.20	7	0.052	2.87
(b)I^-			
22.4	1	0.104	6.92
19.8	2	0.097	6.70
13.9	3	0.087	6.03
11.8	4	0.082	5.69
6.82	5	0.064	4.46
6.12	6	0.061	4.22
2.20	7	0.032	2.16
(c) Co^{2+}			
22.4	1	0.059	4.12
19.8	2	0.057	3.99
13.9	3	0.052	3.59
11.8	4	0.049	3.39
6.82	5	0.038	2.66
6.12	6	0.036	2.51
2.20	7	0.018	1.28

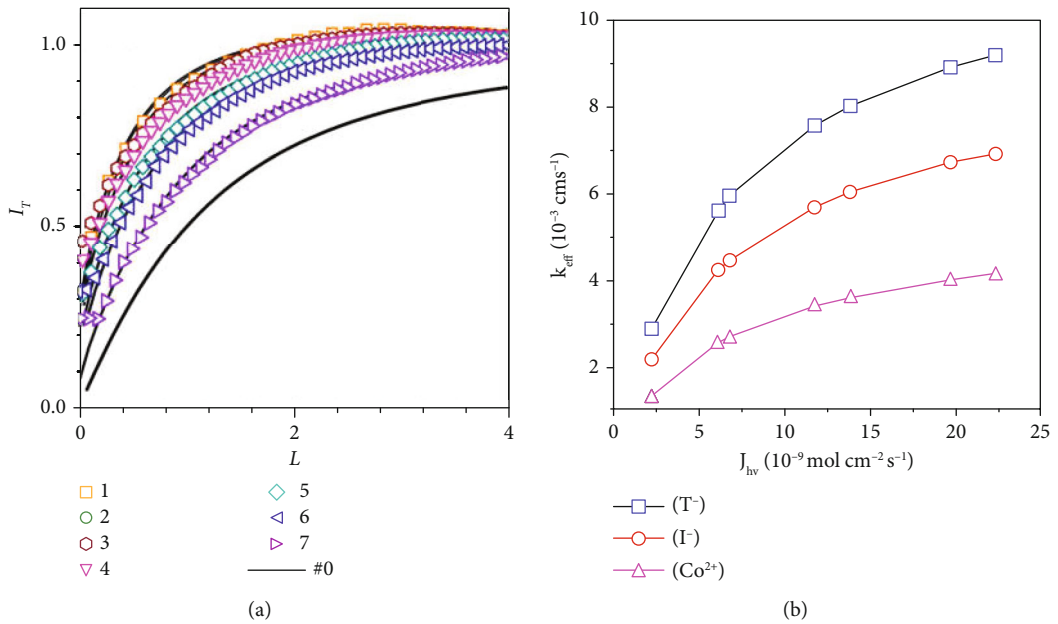

Figure 6: (a) Normalized SECM feedback approach curves of Pt UME towards NiO/P1 with electrolyte T^-. (b) Plot of J_{hv} vs. k_{eff} in three electrolytes (T^-), (I^-), and (Co^{2+}) under the illumination of blue LED.

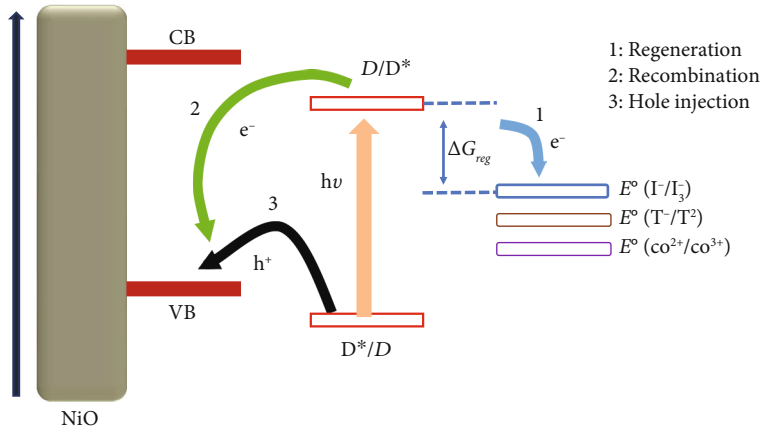

FIGURE 7: Schematic energy level diagram in p-DSSCs for three electrolytes (1) regeneration, (2) recombination, and (3) hole injection.

3.3. SECM Feedback Mode Investigation of NiO/P1 Films in Different Electrolytes. We examined the normalized approach curves of P1/NiO with different electrolytes (I^-, T^-, and Co^{2+}) at varied intensities of blue illumination to demonstrate the dependence of regeneration kinetics on electrochemical characteristics of electrolytes. In the three different electrolytes listed in Table 4, the normalized approach curves of the P1/NiO sample with photon flux density J_{hv} and first-order rate constant k_{eff} were increased, as shown in Figure 6(a).

The SECM approach curves of the electrolytes T^- and Co^{2+} in various intensities are shown in supplementary information in Figure SI-II (a and b). The k_{eff} vs. J_{hv} for the three electrolytes I^-, T^-, and Co^{2+} is shown in Figure 6(b), and Table 2 shows the experimental value of k_{eff} and J_{hv} for each electrolyte. The experimental data demonstrates that k_{eff} calculated value from T^- electrolyte is higher than I^- and Co^{2+}. Between the three electrolytes, however, there were significant differences in both the regeneration rate constant and the absorption cross-section.

Thus, the reduction rate constant k_{red} and excitation cross section Φ_{hv} for the P1/NiO film were evaluated as $k_{red} = 6.8 \times 10^5 mol^{-1}cm^3s^{-1}$, $\Phi_{hv} = 4.93 \times 10^6 mol^{-1}cm^2$ with I^- in blue illumination, $k_{red} = 7.87 \times 10^5 mol^{-1}cm^3s^{-1}$, $\Phi_{hv} = 5.92 \times 10^6 mol^{-1}cm^2$ with T^-, and $k_{red} = 5.72 \times 10^5 mol^{-1}cm^3s^{-1}$, $\Phi_{hv} = 4.73 \times 10^6 mol^{-1}cm^2$ with Co^{2+}. It is noted that observable variation of the reduction rate and absorption cross section with different electrolytes indicates that the regeneration kinetics is dependent on electrolyte and dye. When a sensitized (P1/NiO) sample is illuminated, the excited state dye D^* injects a hole into the NiO semiconductor's valence band (VB), followed by the reduction of the dye D^- as shown in Figure 7. The electrolyte interruption of dye regeneration kinetics at the sensitized semiconductor/electrolyte interfaces is critical to the device operation efficiency of P-DSSCs. The reduction potentials (M/M^-) of I^-/I_3^-, T_2/T^-, and Co^{2+}/Co^{3+} electrolytes were found to be -0.35 V, -0.5 V, and -1.08 V (vs. NHE), respectively [15, 41].

The equation of the driving force for the regeneration reaction of electrolyte [35] is given by

$$\frac{\Delta G_{reg}}{e^-} = \left[E\left(\frac{M}{M^-}\right) - E\left(\frac{D}{D^-}\right)\right], \quad (6)$$

where ΔG_{reg} represents the free energy of the sensitizer's regeneration reaction, $E(D/D-)$ represents the dye's reduction potential, and E(M/M$^-$) represents the mediator's reduction potential. The $E(D/D-)$ for P1 dye was estimated to be -3.93 eV based on our experimental findings [31, 41]. The regeneration energy per elementary charge ($\Delta G_{reg}/e^-$) was calculated to be 2.78eV for I^-/I_3^-, 2.63 eV for T_2/T^-, and 2.05 eV for Co^{2+}/Co^{3+}. However, among the three electrolytes, the regeneration free energy of I^-/I_3^- is significantly higher than T_2/T^- and Co^{2+}/Co^{3+}. As shown in Table 4, the dye regeneration kinetics in the electrolyte (T^-) was faster than in the (I^-) and (Co^{2+}) electrolytes.

As a result, Figure 7 shows a significant variation in the driving force of the P1 dye regeneration reaction with three different electrolytes. To avoid recombination reactions between reduced electrolyte and hole in NiO as $M^- + h^+/VB_{NiO}$, $(D/D^-) > E(M/M^-) > E_{VB}(\text{NiO})$ (where 0.54 V vs. NHE for NiO) is a critical precondition for efficient dye regeneration reaction [31, 41]. As a result, SECM approach curves shows that dye regeneration kinetics are clearly influenced by electrolyte properties and dye nature. The electrolyte's effect as a downcast of the valance band edge hastened the hole injection rate of the excited dye, affecting the driving force of the dye regeneration. The use of SECM feedback modes to characterize dye reduction constants and absorption cross-sections has proven to be an innovative technique. Therefore, the overall SECM investigation opens a new outlook for p-type DSSC characterization.

4. Conclusion

The investigation of dye molecule regeneration kinetics using an electrolyte NiO electrode adds to a better understanding of the dye regeneration mechanism in P-type DSSC liquid electrolytes. Approach curves show that the kinetics of regeneration depends on the wavelength of the incident

light, photon flux density, optical properties of sensitizers, and chemical properties of electrolytes. This study shows a clear variation of regeneration constants such as reduction rate, regeneration rate, absorption cross-section and the free energies (in eV) of the hole injection of sensitized NiO. As a result, the SECM feedback approach has been shown to be a more effective way of exploring the details of charge transfer reaction rates in the development of various P-type DSSC components. Thus, SECM with a feedback model is a novel method for the characterization of regeneration kinetics processes in P-type generation photovoltaics. This allows the straight forward testing of efficient electrolytes and efficient dyes to harvest light energy in photovoltaic systems.

Data Availability

The data used in this study are included in the article. If further information be required, this is available from the corresponding author upon request.

Conflicts of Interest

The authors declare that they have no conflicts of interest.

Acknowledgments

We are grateful for the Ph.D. fellowship provided by the Chinese Scholarship Council (CSC). And, we would also like to thank Prof. Dr. Mingkui Wang and Prof. Dr. Yen Shen for their contributions. The experiments were performed on a CHI920C electrochemical workstation (CH Instruments, Shanghai) provided by the Chinese Scholarship Council (CSC) for Ph.D. fellowship.

Supplementary Materials

* SCEM normalized approach curves of UME towards the C343/NiO and P1/NiO in red illumination are documented in Figure SI-I. *The SECM approach curves of the electrolytes T^- and Co^{2+} in various intensities are shown in supplementary information in Figure SI-II (a and b). *(Supplementary Materials)*

References

[1] B. O'regan and M. Grätzel, "A low-cost, high-efficiency solar cell based on dye-sensitized colloidal TiO2 films," *Nature*, vol. 353, no. 6346, pp. 737–740, 1991.

[2] M. Grätzel, "Solar energy conversion by dye-sensitized photovoltaic cells," *Inorganic Chemistry*, vol. 44, no. 20, pp. 6841–6851, 2005.

[3] M. Grätzel, "Ultrafast colour displays," *Nature*, vol. 409, no. 6820, pp. 575-576, 2001.

[4] M. D. McGehee, "Paradigm shifts in dye-sensitized solar cells," *Science*, vol. 334, no. 6056, pp. 607-608, 2011.

[5] Q. Zhang and G. Cao, "Nanostructured photoelectrodes for dye-sensitized solar cells," *Nano Today*, vol. 6, no. 1, pp. 91–109, 2011.

[6] Q. Zhang, C. S. Dandeneau, X. Zhou, and G. Cao, "ZnO nanostructures for dye-sensitized solar cells," *Advanced Materials*, vol. 21, no. 41, pp. 4087–4108, 2009.

[7] M. K. Nazeeruddin, A. Kay, I. Rodicio et al., "Conversion of light to electricity by cis-X2bis (2, 2'-bipyridyl-4, 4'-dicarboxylate) ruthenium (II) charge-transfer sensitizers (X= Cl-, Br-, I-, CN-, and SCN-) on nanocrystalline titanium dioxide electrodes," *Journal of the American Chemical Society*, vol. 115, no. 14, pp. 6382–6390, 1993.

[8] NREL research cells efficiency chart, 2019, March 2020 http://www.nrel.gov/ncpv/images/efficiency_chart.jpg.

[9] K. Kakiage, Y. Aoyama, T. Yano, K. Oya, J. I. Fujisawa, and M. Hanaya, "Highly-efficient dye-sensitized solar cells with collaborative sensitization by silyl-anchor and carboxy-anchor dyes," *Chemical Communications*, vol. 51, no. 88, pp. 15894–15897, 2015.

[10] J. N. Clifford, E. Palomares, M. K. Nazeeruddin, M. Grätzel, and J. R. Durrant, "Dye dependent regeneration dynamics in dye sensitized nanocrystalline solar cells: evidence for the formation of a ruthenium bipyridyl cation/iodide intermediate," *The Journal of Physical Chemistry C*, vol. 111, no. 17, pp. 6561–6567, 2007.

[11] Y. Tachibana, S. A. Haque, I. P. Mercer, J. R. Durrant, and D. R. Klug, "Electron injection and recombination in dye sensitized nanocrystalline titanium dioxide films: a comparison of ruthenium bipyridyl and porphyrin sensitizer dyes," *The Journal of Physical Chemistry B*, vol. 104, no. 6, pp. 1198–1205, 2000.

[12] E. M. Barea, J. Ortiz, F. J. Payá et al., "Energetic factors governing injection, regeneration and recombination in dye solar cells with phthalocyanine sensitizers," *Energy & Environmental Science*, vol. 3, no. 12, pp. 1985–1994, 2010.

[13] S. A. Haque, Y. Tachibana, D. R. Klug, and J. R. Durrant, "Charge recombination kinetics in dye-sensitized nanocrystalline titanium dioxide films under externally applied bias," *The Journal of Physical Chemistry B*, vol. 102, no. 10, pp. 1745–1749, 1998.

[14] M. K. Kashif, J. C. Axelson, N. W. Duffy et al., "A new direction in dye-sensitized solar cells redox mediator development: in situ fine-tuning of the cobalt (ii)/(iii) redox potential through Lewis base interactions," *Journal of the American Chemical Society*, vol. 134, no. 40, pp. 16646–16653, 2012.

[15] T. Leijtens, I.-K. Ding, T. Giovenzana, J. T. Bloking, M. D. McGehee, and A. Sellinger, "Hole transport materials with low glass transition temperatures and high solubility for application in solidstate dye-sensitized solar cells," *ACS Nano*, vol. 6, no. 2, pp. 1455–1462, 2012.

[16] H. Li, K. Fu, A. Hagfeldt, M. Grätzel, S. G. Mhaisalkar, and A. C. Grimsdale, "A simple 3,4-ethylenedioxythiophene based hole-transporting material for perovskite solar cells," *International Edition*, vol. 53, no. 16, pp. 4085–4088, 2014.

[17] F. Odobel, L. Le Pleux, Y. Pellegrin, and E. Blart, "New photovoltaic devices based on the sensitization of p-type semiconductors: challenges and opportunities," *Accounts of Chemical Research*, vol. 43, no. 8, pp. 1063–1071, 2010.

[18] F. Sahiner, A. K. Ali, S. Denizaltı, Z. Kandemir, and S. Erten-Ela, "Naphthalene imides as novel p-type sensitizers for NiO-based p-type dye-sensitized solar cells," *New Journal of Chemistry*, vol. 44, no. 36, pp. 15526–15537, 2020.

[19] Y. Higashino, S. Erten-Ela, and Y. Kubo, "π -Expanded dibenzo-BODIPY with near-infrared light absorption: Investigation of photosensitizing properties of NiO-based p -type

dye- sensitized solar cells," *Dyes and Pigments*, vol. 170, article 107613, 2019.

[20] A. Y. Anderson, P. R. Barnes, J. R. Durrant, and B. C. O'Regan, "Quantifying regeneration in dye-sensitized solar cells," *The Journal of Physical Chemistry C*, vol. 115, no. 5, pp. 2439–2447, 2011.

[21] T. Daeneke, A. J. Mozer, T. H. Kwon et al., "Dye regeneration and charge recombination in dye-sensitized solar cells with ferrocene derivatives as redox mediators," *Energy & Environmental Science*, vol. 5, no. 5, pp. 7090–7099, 2012.

[22] T. Daeneke, A. J. Mozer, Y. Uemura et al., "Dye regeneration kinetics in dye-sensitized solar cells," *Journal of the American Chemical Society*, vol. 134, no. 41, pp. 16925–16928, 2012.

[23] C. Lee, J. Kwak, and A. J. Bard, "Application of scanning electrochemical microscopy to biological samples," *Proceedings of the National Academy of Sciences*, vol. 87, no. 5, pp. 1740–1743, 1990.

[24] I. Beaulieu, S. Kuss, J. Mauzeroll, and M. Geissler, "Biological scanning electrochemical microscopy and its application to live cell studies," *Analytical Chemistry*, vol. 83, no. 5, pp. 1485–1492, 2011.

[25] K. Szot, W. Nogala, J. Niedziolka-Jönsson et al., "Hydrophilic carbon nanoparticle-laccase thin film electrode for mediatorless dioxygen reduction: SECM activity mapping and application in zinc-dioxygen battery," *Electrochimica Acta*, vol. 54, no. 20, pp. 4620–4625, 2009.

[26] A. Kishi, M. Inoue, and M. Umeda, "Scanning electrochemical microscopy study of H2O2 byproduct during O2 reduction at Pt/C-Nafion composite cathode," *The Journal of Physical Chemistry C*, vol. 114, no. 2, pp. 1110–1116, 2010.

[27] H. Li, R. Liu, W. Kong et al., "Carbon quantum dots with photo-generated proton property as efficient visible light controlled acid catalyst," *Nanoscale*, vol. 6, no. 2, pp. 867–873, 2014.

[28] A. Sumboja, U. M. Tefashe, G. Wittstock, and P. S. Lee, "Monitoring electroactive ions at manganese dioxide pseudocapacitive electrodes with scanning electrochemical microscope for supercapacitor electrodes," *Journal of Power Sources*, vol. 207, pp. 205–211, 2012.

[29] K. C. Huang, J. H. Huang, C. H. Wu et al., "Nanographite/polyaniline composite films as the counter electrodes for dye-sensitized solar cells," *Journal of Materials Chemistry*, vol. 21, no. 28, pp. 10384–10389, 2011.

[30] G. Alemu, J. Li, J. Cui et al., "Investigation on regeneration kinetics at perovskite/oxide interface with scanning electrochemical microscopy," *Journal of Materials Chemistry A*, vol. 3, no. 17, pp. 9216–9222, 2015.

[31] S. Gupta and C. Price, "Scanning electrochemical microscopy of graphene/polymer hybrid thin films as supercapacitors: physical-chemical interfacial processes," *AIP Advances*, vol. 5, no. 10, article 107113, 2015.

[32] S. Choi, D. Shin, and J. Chang, "Nanoscale fiber deposition via surface charge migration at air-to-polymer liquid Interface in near-field electrospinning," *ACS Applied Polymer Materials*, vol. 2, no. 7, pp. 2761–2768, 2020.

[33] F. Li and P. R. Unwin, "Scanning electrochemical microscopy (SECM) of photoinduced electron transfer kinetics at liquid/liquid interfaces," *The Journal of Physical Chemistry C*, vol. 119, no. 8, pp. 4031–4043, 2015.

[34] G. Alemu, J. Cui, K. Cao, J. Li, Y. Shen, and M. Wang, "Investigation of the regeneration kinetics of organic dyes with pyridine ring anchoring groups by scanning electrochemical microscopy," *RSC Advances*, vol. 4, no. 93, pp. 51374–51380, 2014.

[35] E. A. Gibson, L. Le Pleux, J. Fortage et al., "Role of the triiodide/iodide redox couple in dye regeneration in p-type dye-sensitized solar cells," *Langmuir*, vol. 28, no. 15, pp. 6485–6493, 2012.

[36] P. Qin, H. Zhu, T. Edvinsson, G. Boschloo, A. Hagfeldt, and L. Sun, "Design of an organic chromophore for p-type dye-sensitized solar cells," *Journal of the American Chemical Society*, vol. 130, no. 27, pp. 8570-8571, 2008.

[37] P. Qin, M. Linder, T. Brinck, G. Boschloo, A. Hagfeldt, and L. Sun, "High incident photon-to-current conversion efficiency of p-type dye-sensitized solar cells based on NiO and organic chromophores," *Advanced Materials*, vol. 21, no. 29, pp. 2993–2996, 2009.

[38] A. G. Alemu and T. Alemu, "Dye regeneration kinetics of sensitized nickel oxide films under illumination investigated by scanning electrochemical microscopy," *Advances in Materials Physics and Chemistry*, vol. 11, no. 4, pp. 78–92, 2021.

[39] U. MengeshaTefashe, K. Nonomura, N. Vlachopoulos, A. Hagfeldt, and G. Wittstock, "Effect of cation on dye regeneration kinetics of N719-sensitized TiO2 films in acetonitrile-based and ionic-liquid-based electrolytes investigated by scanning electrochemical microscopy," *The Journal of Physical Chemistry C*, vol. 116, no. 6, pp. 4316–4323, 2012.

[40] Y. Shen, U. M. Tefashe, K. Nonomura, T. Loewenstein, D. Schlettwein, and G. Wittstock, "Photoelectrochemical kinetics of eosin Y-sensitized zinc oxide films investigated by scanning electrochemical microscopy under illumination with different LED," *Electrochimicaacta*, vol. 55, no. 2, pp. 458–464, 2009.

[41] U. M. Tefashe, T. Loewenstein, H. Miura, D. Schlettwein, and G. Wittstock, "Scanning electrochemical microscope studies of dye regeneration in indoline (D149)-sensitized ZnO photoelectrochemical cells," *Journal of Electroanalytical Chemistry*, vol. 650, no. 1, pp. 24–30, 2010.

[42] Y. Shen, K. Nonomura, D. Schlettwein, C. Zhao, and G. Wittstock, "Photoelectrochemical kinetics of eosin Y-sensitized zinc oxide films investigated by scanning electrochemical *microscopy*," *European Journal*, vol. 12, no. 22, pp. 5832–5839, 2006.

[43] A. Getachew Alemu, "Dye regeneration kinetics of C343-sensitized nickel oxide investigated by scanning electrochemical microscopy," *Materials Sciences and Applications*, vol. 13, no. 1, pp. 22–38, 2022.

[44] G. Alemu, B. Zhang, J. Li et al., "Investigation of dye-regeneration kinetics at dyesensitized p-type CuCrO 2 film/electrolytes interface with scanning electrochemical microscopy," *Nano*, vol. 9, no. 5, p. 1440008, 2014.

[45] D. Karthik, K. J. Thomas, J. H. Jou, and Y. L. Chen, "Synthesis, characterization and electroluminescence of carbazole-benzimidazole hybrids with thiophene/phenyl linker," *Dyes and Pigments*, vol. 133, pp. 132–142, 2016.